ACS APPLIED MATERIALS & INTERFACES

Research Article

www.acsami.org

Complexation-Tailored Morphology of Asymmetric Block Copolymer Membranes

Poornima Madhavan,[†] Klaus-Viktor Peinemann,[‡] and Suzana P. Nunes*[,†]

[†]Water Desalination and Reuse Center and [‡]Advanced Membranes and Porous Materials, King Abdullah University of Science and Technology, 23955-6900 Thuwal, Saudi Arabia

Supporting Information

ABSTRACT: Hydrogen-bond formation between polystyrene-*b*-poly (4-vinylpyridine) (PS-*b*-P4VP) block copolymer (BCP) and −OH/−COOH functionalized organic molecules was used to tune morphology of asymmetric nanoporous membranes prepared by simultaneous self-assembly and nonsolvent induced phase separation. The morphologies were characterized by field emmision scanning electron microscopy (FESEM) and atomic force microscopy (AFM). Hydrogen bonds were confirmed by infrared (IR), and the results were correlated to rheology characterization. The OH-functionalized organic molecules direct the morphology into hexagonal order. COOH-functionalized molecules led to both lamellar and hexagonal structures. Micelle formation in solutions and their sizes were determined using dynamic light scattering (DLS) measurements and water fluxes of 600−3200 L/m^2·h·bar were obtained. The pore size of the plain BCP membrane was smaller than with additives. The following series of additives led to pores with hexagonal order with increasing pore size: terephthalic acid (COOH-bifunctionalized) < rutin (OH-multifunctionalized) < 9-anthracenemethanol (OH-monofunctionalized) < 3,5-dihydroxybenzyl alcohol (OH-trifunctionalized).

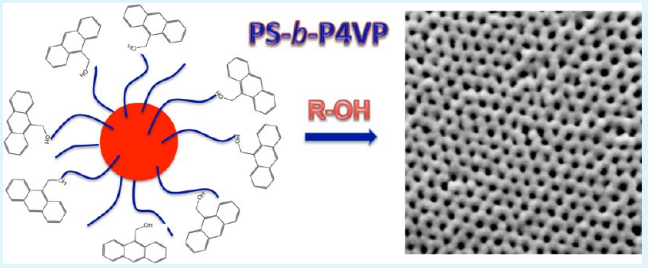

KEYWORDS: *hydrogen bond, self-assembly, membranes, block copolymers*

INTRODUCTION

The self-assembly of block copolymers (BCPs) has gained increasing importance for applications such as membranes, templates, and lithography.[1−3] The equilibrium morphology in the bulk is controlled by the thermodynamic interaction between blocks as well as their degree of polymerization. In solution, the block interaction with solvents is an additional very important parameter. In selective solvents different morphologies such as spherical micelles, vesicles, wormlike aggregates, gyroids, lamellas, and cylinders[4−11] can be observed. Efforts have been made to search for new routes to tune the morphologies of block copolymer self-assembly by chemically modifying one of the blocks of BCP,[12] changing the pH,[13] addition of complex forming metal salt,[14] homopolymers and small molecules acting as surfactants, which form hydrogen-bonds with one of the copolymer blocks.[15−17] Complex formation with metal salts (coordination) and small organic molecules (hydrogen-bond formation) is reported to be particularly effective in controlling the morphology[18−20] of thin films. In this way supramolecular chemistry can tune the morphology without the burden of synthesizing completely new families of BCPs. Small organic molecules can be also washed away as a strategy to form nanoporous structures.[21]

Varieties of block copolymers are readily available. Polystyrene-*b*-poly (4-vinylpyridine) (PS-*b*-P4VP) is convenient for supramolecular self-assembly, since the basic pyridine groups easily complex with metal salts or hydrogen donor organic molecules containing −OH, —COOH groups. Ten Brinke, Ikkala, and co-workers[22−24] are pioneering in supramolecular assembly of BCP with addition of small organic molecules to tune their morphology in solution and in bulk. Our interest is to use analogous supramolecular techniques to form nanoporous block copolymer membranes by phase inversion technique, i.e. by solution casting and immersion in water. We previously demonstrated that nanoporous block copolymer membranes could be obtained with exceptionally high selectivity and high flux, resulting from narrow pore size distribution and a high pore density, respectively.[25−28] The method is easily scalable, in one step, without need for post-treatment like block etching or additive postextraction. We have been working on understanding the mechanism of pore formation involved and optimizing the manufacturing process to ensure reproducibility with long-range order.[26−28] Figure 1 shows a simplified scheme of how micelles assemble in solution to give rise to regular pores. We recently reported a detailed investigation on the mechanism of pore formation in block copolymer membranes by phase inversion with the help of small-angle scattering and modeling.[29] Although it is possible to achieve long-range order, by tuning the solvent mixture, the addition of complexing agents is expected to facilitate and

Received: April 23, 2013
Accepted: July 1, 2013
Published: July 1, 2013

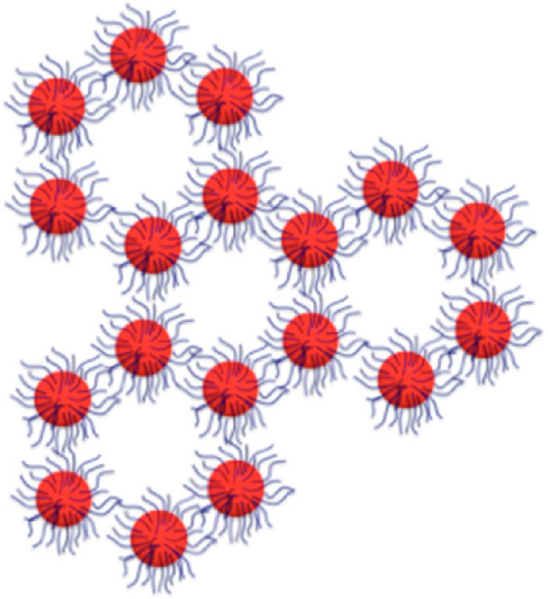

Figure 1. Micelle assembly for formation of hexagonal pores in block copolymer membranes (adapted from ref 27)

stabilize the assembly and/or induce different morphologies. We have reported that metal complexation with PS-*b*-P4VP allows generation of isoporous membranes by nonsolvent induced phase separation[28] even with solvent mixtures and copolymer concentrations, which would not lead to ordered morphology. The degree of order is a function of the different cations used such as Cu^{2+}, Ni^{2+}, Co^{2+}, and Fe^{2+} and of the pyridine−metal complex stability constant. We believe that the cations intensify the intermicellar links and stabilize the order before immersion in water. We also recently demonstrated that isoporous membranes prepared from block copolymer could be used for challenging tasks like the separation of bovine serum albumin and hemoglobulin, proteins with very similar molecular weights.[30] Extending the application to other biological macromolecules would require membranes with other pore sizes. A potential strategy for pore size control is to change the block size and therefore the micelle dimensions, which are involved in the assembly and pore formation. A challenge is to tune pore size in an even simpler way, which this is the main motivation of this work. By a systematic investigation we demonstrated that organic molecules containing mono-, di-, tri-, and polyhydroxyl/acids functional groups strongly interact with the pyridine block of PS-*b*-P4VP, leading to morphology diversification and controlled membrane pore size.

EXPERIMENTAL SECTION

Materials. Polystyrene-*b*-poly(4-vinylpyridine) block copolymer P10900-S4VP (PS-*b*-P4VP 188 000-*b*-64 000 g/mol) was purchased from Polymer Source, Inc., Canada. Dimethyl formamide (DMF) was supplied by Fisher Scientific; Rutin (Ru) was supplied by Acros organics and used without further purification. 3,5-Dihydroxybenzyl alcohol (DHBA), 9-anthracenemethanol (AM), mellitic acid (MA), terephthalic acid (TPA), 1,3,5-tris(4′carboxy[1,1′-biphenyl]-4-yl) benzene (Tris), and tetrahydrofuran (THF) were purchased from Sigma-Aldrich and used as received.

Membrane Preparation. All the membranes were prepared using a solution containing 18 wt % block copolymer (BCP) in a mixture of 50 wt % DMF and 32 wt% THF. Different organic molecules were mixed to the solution and stirred at room temperature for 24 h. The BCP solutions were cast on a glass plate using a casting knife with 200 μm air gap. The solvent was allowed to evaporate for up to 10 s, and the film was immersed in water at room temperature followed by drying at 60 °C for 24 h for infrared (IR) and differential scanning calorimetry (DSC) analysis.

Attenuated Total Reflectence Fourier Transform Infrared (ATR-FTIR). A Perkin-Elmer 100 ATR-FTIR spectrometer was used for recording the IR spectra of block copolymer membrane. Data were collected over 16 scans with a resolution of 4 cm^{-1}. The ATR-FTIR measurements were made at room temperature, using an ATR unit at a nominal incident angle of 45°.

Scanning Electron Microscopy. Micrographs of membranes were obtained using a FEI Quanta 200 Field Emission Scanning Electron Microscope. Imaging was carried out at 5 kV with a working distance of 10 mm. The membrane samples were mounted on aluminum stubs using aluminum tape and Au coated before imaging for 45 s at 20 mA.

Atomic Force Microscopy. AFM analysis was performed using an ICON Veeco microscope in tapping mode. The tip characteristics are as follows: spring constant 3 N m^{-1}, resonant frequency 60−80 Hz. Block copolymer membranes were dried, and a small piece of membrane was imaged directly.

Rheology. Rheological measurements were carried out at 25 °C with AR- 1500 ES Rheometer with a cone and plate fixture of diameter 25 mm and a cone angle of 1°. The rheology measurements were performed in the linear viscoelastic region. The range of shear rates used for the viscosity measurements is 10−1000 s^{-1}.

Dynamic Light Scattering (DLS). DLS measurements were taken with a Malvern Zetasizer Nano Series (nano-ZS) at room temperature. Solutions of 0.1 g/L PS-*b*-P4VP with various weight percent of −OH and −COOH molecules in DMF/THF solvent mixtures were investigated.

Water Flux Measurement. Pure water fluxes of membranes were measured using a stirred Amicon dead-end ultrafilitration cell at 1 bar. The membranes for flux measurements were prepared on a nonwoven polyester support. Effective membrane area was 5 cm^2. Deionized water was used for water flux measurements.

RESULTS AND DISCUSSION

The organic molecules bearing −OH and −COOH functional groups in Schemes 1 and 2 have been used for complex formation with PS-*b*-P4VP block copolymer and membrane formation.

We have demonstrated that the complexation of P4VP blocks with metals such as Cu, Ni, Fe, and Co could be used to guide the formation of ordered nanoporous membranes.[27,28]

Scheme 1. OH-Bearing Organic Molecules for Supramolecular Self-Assembly with PS-*b*-P4VP

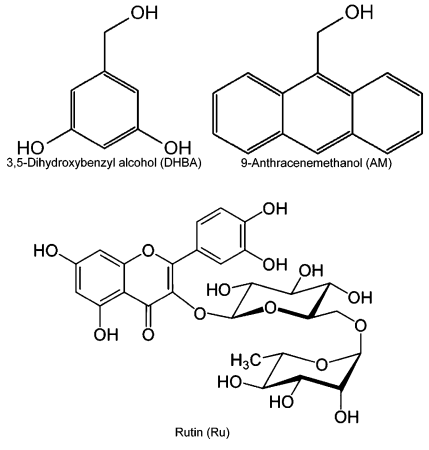

dx.doi.org/10.1021/am401497m | ACS Appl. Mater. Interfaces 2013, 5, 7152−7159

Scheme 2. COOH-Bearing Organic Molecules Used for Supramolecular Self-Assembly with PS-*b*-P4VP

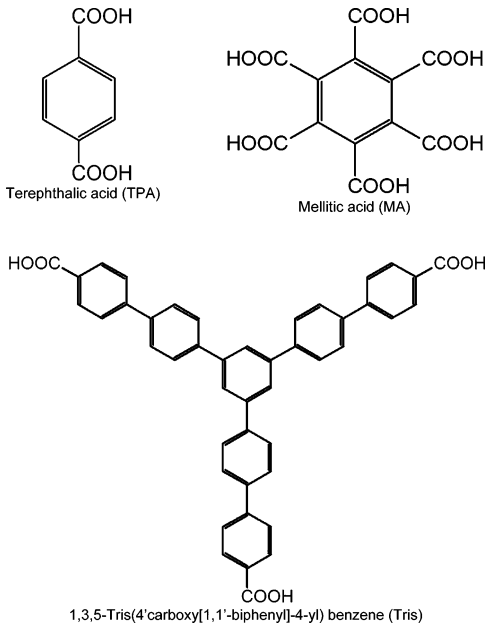

Small organic molecules with a strong tendency of forming hydrogen bonds and/or favoring acid–base complexation[6,24] have been proposed by different groups to guide the nanostructuring of block copolymer systems. Van Zoelen et al.[24] used the strong interaction of pentadecylphenol and pyridine to induce the formation of nanorods. Hayward and Pochan[6] used multiamines to tailor assemblies of poly(acrylic acids). The amines are able to redefine micelle geometries and introduce long-range interactions. Complexation of P4VP-containing block copolymers with small molecules like naphtol, naphtoic acid, and 1-pyrenebutyric acid, perfluorooctanoic acid, which contain hydrogen donor groups, has been explored to prepare nanostructured dense BCP thin film by dip coating.[31−33] Here, we propose an analogous strategy, using different molecules to direct the morphology of nanoporous membranes manufactured by combining phase inversion and block copolymer self-assembly. We focused on two classes of molecules: with −COOH and −OH groups as in Schemes 1 and 2. Organic molecules such as Rutin (3 wt %), DHBA (6 wt %), MA (6 wt %), TPA (3 wt %), Tris (6 wt %), and AM (6 wt %) were blended with PS-*b*-P4VP in solution for hydrogen bond formation. The organic molecules were added to the BCP solution and stirred for 24 h at room temperature. The copolymer composition (18 wt %) and solvents were kept constant for all casting solutions. The amounts of added organic molecules were mostly 6 wt %, but for Rutin and TPA only a maximum of 3 wt % could be added without precipitation. The solutions were cast on a glass plate or polyester nonwoven, evaporated for 10 s, and immersed in water for phase inversion. When immersed in water, solvent–water exchange occurs. The solvent in the BCP solution migrates to water and the water penetrates into the incipient membrane solution to create the pores on the top surface of membrane. Phase separation proceeds, and the porous substructure of the membrane is then formed.

To study the hydrogen bonding behavior and morphology of membrane, pure BCP solutions were cast and manufactured into membranes under the same condition and compared with those obtained in the presence of different organic molecules.

ATR-FTIR Characterization. Chemical structure and hydrogen bond formation between PS-*b*-P4VP and −OH/COOH containing organic molecules were investigated using IR spectroscopy. Figure 2 shows the IR spectra range with peaks, which are relevant for hydrogen bonds.

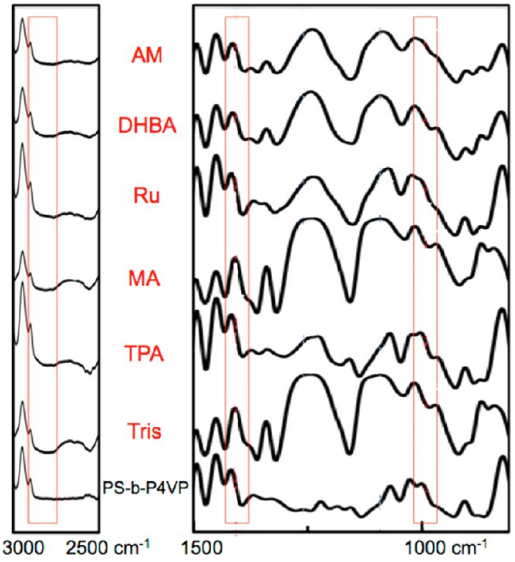

Figure 2. ATR-FTIR spectra for PS-*b*-P4VP nanostructured membranes (plain membranes and membranes with different additives).

An absorption band at 995 cm^{-1} corresponds to the free pyridine group, observed in pure BCP membrane. This peak shifted to 1013 cm^{-1} after the formation of H-bonds with proton donor groups. This is evident for Tris, MA, TPA (less than for the first two) and for DHBA. For AM and Ru, practically no change can be seen. An absorption peak near 1415 cm^{-1}, for the plain membranes is characteristic of unbounded pyridine. The peak is broadened and slightly shifted to 1419 cm^{-1} after hydrogen bond formation between pyridine and the hydrogen-donor groups. The change in the peak again is more accentuated for Tris and MA. The appearance of a broad absorption band at 2550 cm^{-1} for BCP solutions with acid functionalized organic molecules indicates the presence of hydrogen bonding between the acid functional group and the pyridine moiety of the BCP. Additional absorption bands (not all shown in Figure 2) are present at 2153, 1715, 1340, 1238, 1095 cm^{-1} for membranes formed from solutions with small organic molecules. This indicates that after the phase inversion process, the additives are still strongly bonded and are not completely washed out of the membrane.

Both Tris and MA are functionalized with at least three COOH groups, which are symmetrically placed in the molecule. Hydrogen-bonds formation[34−36] depends on the strength of the proton donors and acceptors and the effectiveness of the complex formation between different molecules depends also on the steric position of the proton donor group as well as the preference to intermolecular hydrogen bonds compared to intramolecular ones. Intramolecular bonds are for instance preferred if six-membered-rings could be formed. The preference for intermolecular hydrogen bonds instead of intramolecular dimers is the key for

dx.doi.org/10.1021/am401497m | ACS Appl. Mater. Interfaces 2013, 5, 7152−7159

building cocrystals of small molecules. Carboxylic acid-pyridine H-bonds play an important role in the formation of pharmaceutical cocrystals designed by supramolecular chemistry and crystal engineering.[36,37] Carboxylic acid moieties are among the most frequent in supramolecular synthons,[36,37] which include self-associated systems like dimers and hetero associations (heterosynthons) composed of complementary functional groups. The analysis of crystal structures containing carboxylic acids in the presence of molecules, containing basic nitrogen atoms as part of a delocalized or conjugated system, demonstrates 98% preference for supramolecular heterosynthons. The requirements for complexation with a pyridine block to guide the copolymer assembly in our work are analogous and COOH-functionalized molecules showed to be excellent additives with strong hydrogen bonds confirmed by FTIR. Alcohols are similar to carboxylic acids as they both can be a hydrogen bond donor or acceptor, depending on the complementary moiety. With pyridine they both act as proton donor. In the presence of basic nitrogens like in pyridine at least 50% of supramolecular heterosynthons (78% in the absence of other proton donors) are formed instead of homosynthons. Although less effective than COOH-functionalized molecules, those bearing OH groups have been also reported to affect self-assembly.[33] In a recent paper, cyclodextrine was used to optimize the morphology of PS-*b*-P4VP porous films.[38] The IR spectra analysis of the systems investigated here indicates that the most effective hydrogen-bond among the OH-functionalized molecules is DABH. The molecule contains three OH groups, which are symmetrically placed, facilitating the interaction with different pyridine groups. AM on the other hand is monofunctional and therefore not appropriate as a linker between 2 pyridine blocks.

Membrane Morphology. Field emission scanning electron micrographs (FESEM) and topographic atomic force micrographs (AFM) are shown in Figures 3 and 4 for membranes prepared by complexation of hydroxyl functionalized organic molecules and block copolymers, followed by phase inversion in water. The solvent composition and polymer weight proportion for all membranes were maintained the same (18 wt % copolymer). Figure 3a represents the surface of the pure PS-*b*-P4VP membrane with no significant order. Figure 3b–d shows membranes with complexing agents as additives. Cross-section FESEM images are shown in Figure S1, as Supporting Information. PS-*b*-P4VP(DHAB), PS-*b*-P4VP(Ru), and PS-*b*-P4VP(AM) have hexagonal ordered pores. With anthracene methanol (AM), the order is the most pronounced. The hexagonal morphology could be better confirmed by AFM. AM, being monofunctional, has no possibility of linking two different pyridine groups. However it can decrease the flexibility of the P4VP segments. We have demonstrated that when we combine BCP self-assembly phase separation in water, the mechanism of pore formation involves BCP micelles formation and their supramolecular assembly.[26,27,39] In the presence of AM, the P4VP-rich corona might become less deformable than without AM. Rigid spherical micelles are better ordered.[26] At the same time, the inclusion of AM in the corona increases the intermicellar distance and as a consequence the pores are larger than in the plain membrane.

Membranes from BCP complexed with the bulkier and less symmetric Rutin molecules are more porous than the pure BCP membrane but the order is lower than AM-BCP membranes. DHAB-complexed BCP membranes are highly porous, the order is confirmed by FESEM and AFM, but FESEM images

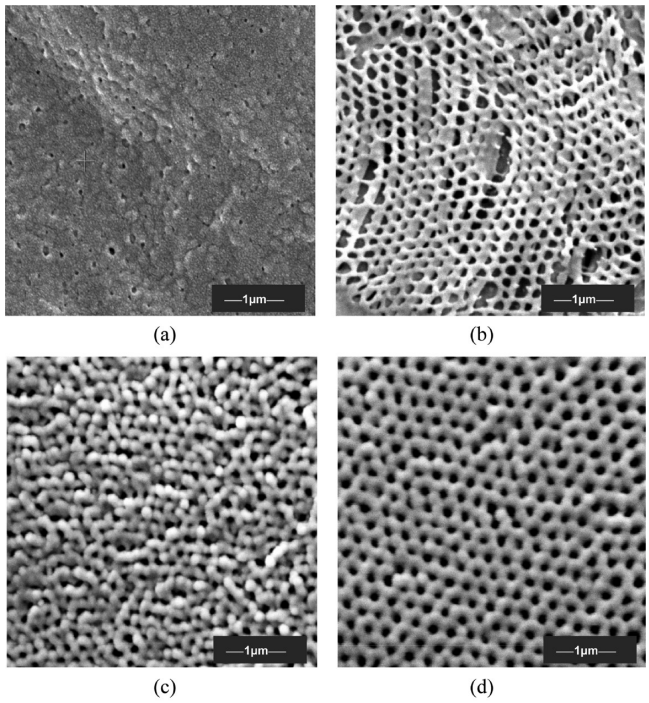

Figure 3. FESEM images of PS-*b*-P4VP nanostructured membrane: (a) pure PS-*b*-P4VP, (b) PS-*b*-P4VP (6 wt % DHBA), (c) PS-*b*-P4VP (3 wt % Ru), (d) PS-*b*-P4VP (6 wt % AM).

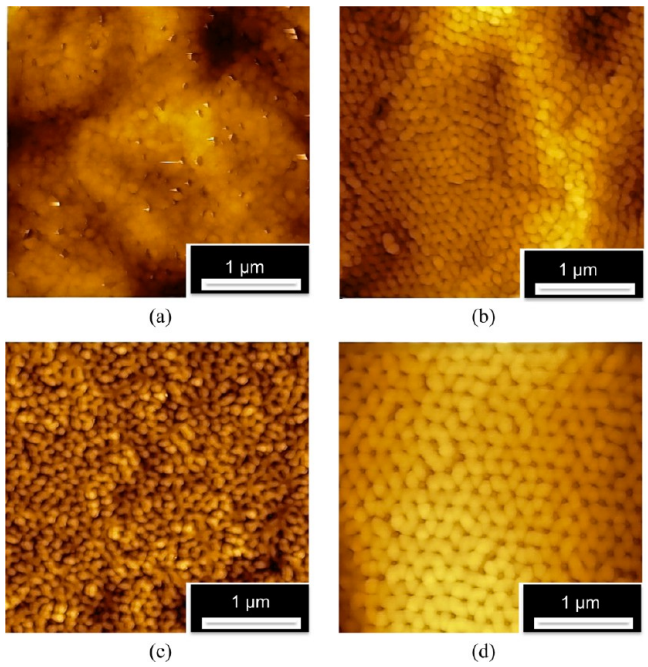

Figure 4. AFM images of PS-*b*-P4VP nanostructured membrane: (a) pure PS-*b*-P4VP, (b) PS-*b*-P4VP (6 wt % DHBA), (c) PS-*b*-P4VP (3 wt % Ru), (d) PS-*b*-P4VP (6 wt % AM).

indicate that the assembly might have a preferential stability in one direction. Pores are larger than for the other OH-additives and certainly larger than in the plain membrane.

The surfaces of membranes prepared from block copolymer solutions with COOH-functionalized organic molecules are shown in Figures 5 (FESEM) and 6 (AFM). Cross-section FESEM images are shown in Figure S1, as Supporting

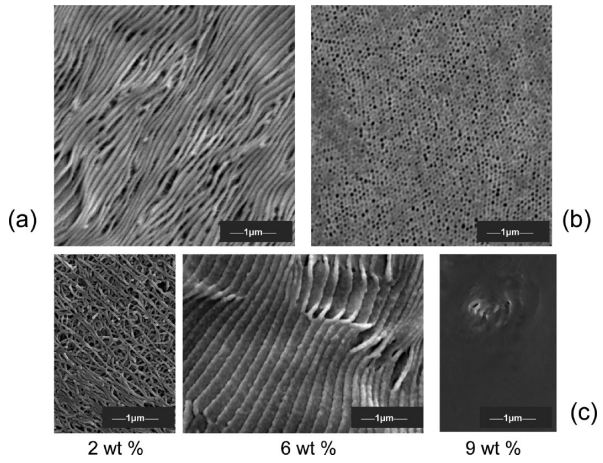

Figure 5. FESEM images of PS-*b*-P4VP nanostructured membrane: (a) PS-*b*-P4VP (6 wt % Tris), (b) PS-*b*-P4VP (3 wt % TPA), and (c) PS-*b*-P4VP (2, 6, and 9 wt % MA).

Information. Tris and MA led to lamellar morphology. In Figure 5c, the influence of the additive concentration can be observed. Excessively high concentration practically eliminates the pores. A clear porosity reduction was observed also when the DHBA concentration was increased to 9 wt % (Supporting Information Figure S2). The membrane prepared with TPA has very ordered hexagonal pores with high porosity and small pore sizes. With this result we can report that while using the same block copolymer, the pore size of the manufactured membrane and the order of the pore morphology can be increased by changing the hydrogen donor additive in the following series:

- Pore size of plain BCP membrane < TPA < Ru < AM < DHBA
- Order of plain BCP membrane < Ru < DHBA < TPA = AM

Roland et al.[33] reported the morphology of PS-*b*-P4VP block copolymer thin-film prepared by dip coating in the presence of naphtol and naphthoic acid. In that case the solution was prepared in tetrahydrofuran, which was completely evaporated to form the solid film. They reported preferential dot morphology when 1-naphthol is used and stripes when acid is the additive; however, the morphology depends also on the coating rate, stripes observed for rapid and thinner coatings. We work with 32 wt % THF:50 wt % DMF mixtures. DMF is a polar (solubility parameter closer to P4VP than to PS, favoring PS cores) low-volatile solvent. The solution layers are much thicker (>100 μm) than those used in dip coating and practically independent of substrate wetting influence. A fast solvent−water exchange is promoted, by immersion in water and the morphology is frozen, remaining much closer to that in the solution. According to previous evidence,[26−28] supramolecular micelle assembly is an essential step in the pore formation of self-assembly/phase inversion membranes. Micelles are favored in the presence of all OH-additives and TPA.

On the other hand, the addition of MA and Tris led to films with lamellar or cylindrical structure (parallel to the surface).

The hydrodynamic radii of PS-*b*-P4VP micelles in dilute solutions with different hydrogen-donor molecules were determined by dynamic light scattering. For DLS measurement DMF/THF solvent mixtures with 50:32 weight ratios were used, analogously to the copolymer membrane casting solution. The copolymer concentration for DLS measurements needs to be much lower (1.0 g /L) than that used for membrane preparation (18 wt %). Light scattering data suggests that micelles are formed in all measured BCP solutions in THF/DMF. The *z*-average value of pure BCP micelle radius in the mixed solvent was 8.1 ± 0.2 nm. In BCP solutions with Ru, DHBA, AM, and TPA, the *z*-average values were 8.1, 8.7, 8.3, and 8.3 nm, respectively, practically nondistinguishable. In the solutions containing hydrogen-donor molecules, which led to lamella morphology (Tris and MA) *z*-average values for micelle radius are higher than without additive. The *z*-average value for Tris is 16.3 nm and for MA is 25.2 nm, respectively, 2 and 3 times higher than for the plain block copolymer in solution.

It can be concluded that compact micelles favor the hexagonal order and pore morphology shown in Figure 3 and 5c. Light scattering data clearly indicates that the addition of organic molecules changes the micelle sizes in solution. The micelle radius size in solutions with Tris and MA are 2- and 3-fold that for copolymers without additives, respectively, indicating that 2 or 3 micelles might be strongly linked or merged. The multifunctional COOH-molecules could facilitate it. Additionally the interaction of the acid molecules with pyridine groups could be strong enough to at least partially protonate them and promote a stretching of the P4VP block.

The hydrogen bond formation between organic molecules and pyridine affects the solution viscosity and therefore also the membrane formation and final morphology. Figure 7 shows how the viscosity changes with the additive incorporation. In all cases the solutions are shear-thinning, indicating that as soon as shear is applied to the ordered assemblies, the interactions between micelles can be disturbed, facilitating the flow. Solutions with mellitic acid (MA), which has six symmetric

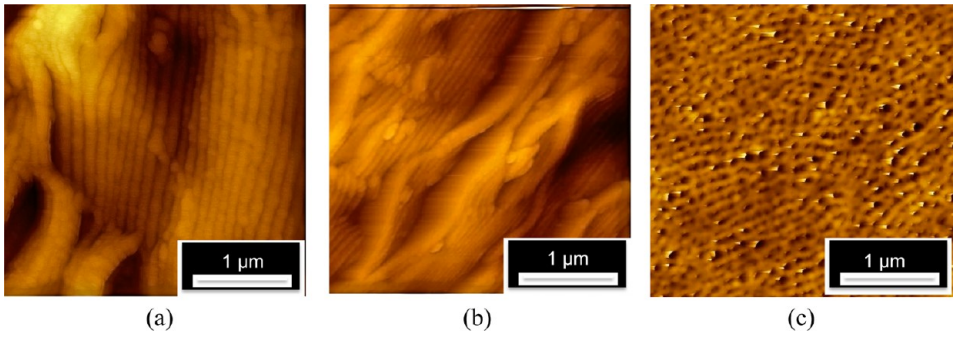

Figure 6. AFM images of PS-*b*-P4VP nanostructured membrane: (a) PS-*b*-P4VP (6 wt % Tris), (b) PS-*b*-P4VP (3 wt % TPA), (c) PS-*b*-P4VP (6 wt % MA).

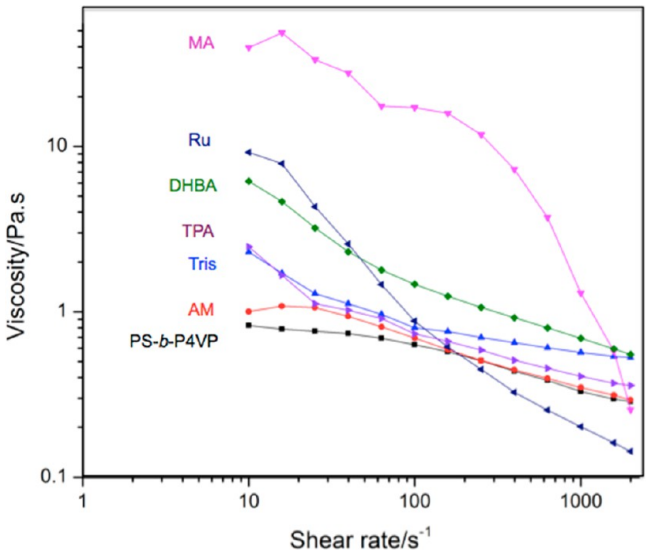

Figure 7. Viscosity of PS-*b*-P4VP solutions with different small organic additives

COOH groups available for interaction with pyridine sites, are those with the highest viscosity, distinguishing from the others. The same system led to a micelle radius 3-fold larger than others and led also to final lamellar structure, in opposite to most other investigated systems. The multi-COOH functionality certainly facilitates intermolecular and intermicellar linking, causing the increase of viscosity. The second system (Tris), which leads to lamellar structure, however, did not substantially distinguish from others, regarding viscosity. The effect of different additives becomes evident in oscillating measurements by taking in account the storage (G') and loss (G'') moduli as a function of the strain amplitude at a fixed frequency. There is detailed investigation in the literature on rheology of water-soluble copolymers with poly(ethylene oxide) blocks.[40,41] Their behavior in semidiluted solution was a starting point for us to understand the micelle rheology in our system as well as results reported by Buitenhuis and Förster[42] for PS-*b*-P4VP in toluene. Toluene is a better solvent for PS and induces micelle formation with a P4VP core, in opposite to the DMF/THF solvent mixture chosen here. For the 188 000-*b*-64 000 g/mol PS-*b*-P4VP system investigated here, "crew cut" micelles with P4VP corona are expected in a 50 (wt %) DMF/32 (wt %) THF solvent mixture. Figure 8 shows the dependence of G' and G'' on strain. Below 65% strain, G' is higher than G'', indicating a strong elastic contribution, typical of soft and hard gels. This is the result of closely packed micelle assemblies, which have been confirmed by SAXS before.[29] As the strain increases, G' and G'' are constant up to 10%. G' decreases. A strain overshoot is observed for G'', indicating break up of the network. Above 65% a strain thinning is observed due to the possibility of layers sliding with the flow direction. The viscous contribution to the flow predominates, and the system behaves like a sol with $G' < G''$. A scheme representing the transition is proposed in Figure 8. A similar behavior was observed for solutions containing different additives, except for 9-anthracenemethanol (AM) and mellitic acid (MA), as summarized in Table 1. The elastic contribution, reflected by G', is larger for terephtalic acid (TPA) and 1,3,5-tris(4′carboxy[1,1′-biphenyl]-4-yl) benzene (Tris) than for the plain copolymer solution. Strong hydrogen bonds were

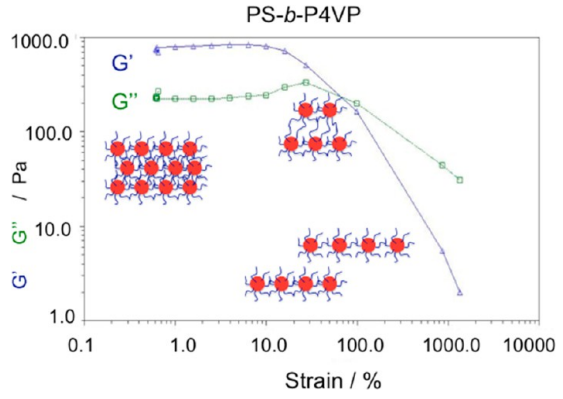

Figure 8. Storage (G') and loss (G'') moduli as a function of strain (%) at 1 Hz for a 18 wt % PS-*b*-P4VP solution in 50 wt % DMF and 32 wt % THF. Scheme of the corresponding micelle assembly in different stages.

Table 1. Values of Storage (G') and Loss (G'') Moduli at Low Strain for 18 wt % Solution of PS-*b*-P4VP in DMF/THF with Different Additives[a]

additive	G' (Pa) at low strain	G'' (Pa) at low strain	strain (%) at $G' = G''$
no	800	200	65
Ru	300	80	50
AM	<20	<20	
DHBA	300	90	50
TPA	900	220	70
Tris	1000	350	60
MA	380	280	----

[a]Strain percent at the crossing point between the G'' and G' curves.

confirmed by IR (Figure 2) for the two systems. They contribute to increase the intermicellar linking and stabilize the gel. This is an important aspect to maintain the assembly order during the immersion in water, during the membrane manufacture.

Although MA forms also strong hydrogen bonds to pyridine and led to copolymer solutions with higher viscosity than the others, G' and G'' were relatively low and not far from each other (Figure 9). As the strain amplitude decreases, both decrease and G' continues to be slightly larger than G''. An explanation for it is shown in Figure 9. The multifunctionality

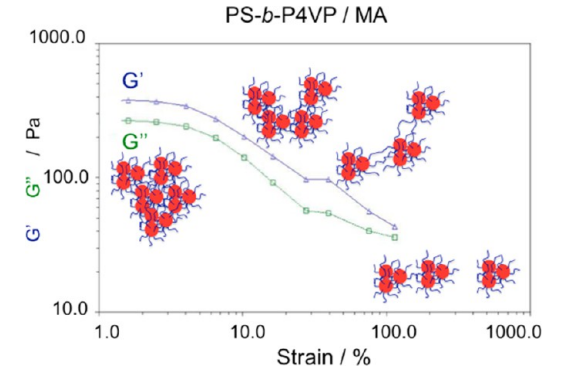

Figure 9. Storage (G') and loss (G'') moduli as a function of strain (%) at 1 Hz for a 18 wt % PS-*b*-P4VP solution in 50 wt % DMF and 32 wt % THF with mellitic acid. Scheme of the corresponding micelle assembly in different stages.

dx.doi.org/10.1021/am401497m | ACS Appl. Mater. Interfaces 2013, 5, 7152−7159

of MA allows the formation of a large number of hydrogen bonds. Strong intra- and intermicellar linking lead to the formation of aggregates, and the system is metastable. The solution is visually milky. The large aggregates are not strongly linked to form a strong network. As the strain is increased, the connection between the large aggregates is broken, and they are progressively aligned with the flow direction.

A different behavior was observed for solutions with AM. The monofunctional molecule forms hydrogen bonds with pyridine, which becomes less available to interact with segments of another micelle. The intercorona link decreases, G' and G'' are similar, and the elasticity of the gel is low (Figure 10). At

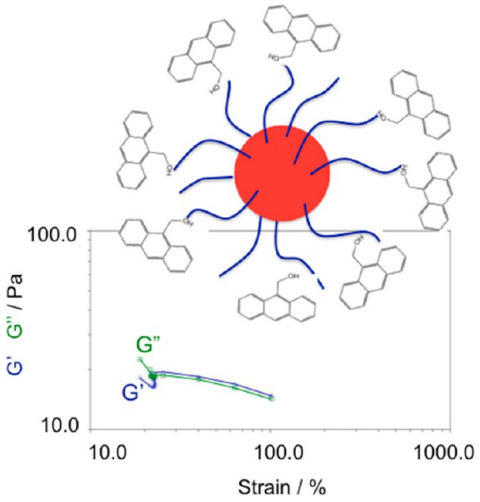

Figure 10. Storage (G') and loss (G'') moduli as a function of strain (%) at 1 Hz for a 18 wt % PS-*b*-P4VP solution in 50 wt % DMF and 32 wt % THF with 9-anthracene methanol (AM). Micelle surrounded by AM molecules forming hydrogen-bonds to pyridine groups in the corona.

the same time the rigid anthracene units make the membrane less deformable and lead to a very uniform morphology (Figures 3d and 4d). The bulky anthracene moieties might also stretch the corona segments and/or be partially dissolved in the PS core. A swollen ordered morphology can be seen by microscopy and larger pores are formed.

Water Flux Measurement and Retention. Water flux measurements were carried out using an Amicon ultrafiltration under 1 bar N_2 gas pressure. Table 1 reports the water flux of pure PS-*b*-PVP membrane and those with complexing organic molecule. All the membranes had a high water flux between 600 and 3200 L/m^2·h·bar.

Table 2. Water Flux and Retention of Membranes Prepared from PS-*b*-P4VP Solutions with Different Additives

additive	water flux (10^3 L/m^2·h·bar)	albumin retention (%)
no	1.2 ± 0.2	
DHBA (OH)	0.6 ± 0.2	
AM (OH)	1.8 ± 0.2	26 ± 2
Ru (OH)	3.2 ± 0.2	
TPA (COOH)	1.2 ± 0.2	62 ± 2
Tris (COOH, lamella)	1.6 ± 0.2	5 ± 2
MA (COOH, lamella)	3.0 ± 0.2	

The water flux did not follow a trend or correlation to the structure on the membrane top layer. The lamellar structured BCP membranes such as PS-*b*-P4VP (MA) and PS-*b*-P4VP (Tris) had fluxes of 3000 and 1600 L/m^2·h·bar. Membranes with hexagonal order had water flux from 600 to 3200 L/m^2·h·bar. The retention of bovine albumin (molecular weight 66 000 g/mol) was measured, by filtering the protein solution and analyzing UV absorption. The lamellar-structured membranes (Tris) had the lowest retention (5%). The elongated pores are not selective enough. The retention is more than 5-fold higher (26%) for (AM) membranes. Both AM and TPA led to pores with hexagonal order. (TPA) membrane pores are clearly smaller (Figure 3d and 5c) than those of (AM) membranes. TPA membranes are able to retain 62% of albumin. The retention of gamma-globulin (molecular weight 150 000 g/mol) was 94% for AM membranes, while for the lamellar Tris it was only 15%. Therefore, we confirm that the membranes with hexagonal pore morphology are much more selective than those with lamellar order, while still keeping very high flux. Probably due to the rigidity of the corona, the resulting pores of the AM membrane are not only very uniform; they are less deformable than in the case of other membranes. This contributes to the high separation factor for globulin/albumin.

CONCLUSIONS

We showed that a small amount of proton-donor organic molecules interferes with the supramolecular assembly of block copolymers in solution and changes the final membrane morphology. OH-functionalized organic molecules tuned the final membrane morphology into hexagonal order. The light scattering data revealed that the sizes of BCP micelles radius formed in solution under the influence of OH group, bearing organic molecules, are around 8 nm. DLS measurements for BCP micelles formed in the presence of COOH-group were up to 3-fold larger than with OH-molecules. A detailed analysis of the system rheology was discussed. The COOH-system with larger micelles aligns in a lamellar structure. Hydrogen bond formation between P4VP and −OH/−COOH groups were confirmed in the final membrane using ATR-FTIR spectroscopy technique. The water fluxes were as high as 3000 L/m^2·h·bar. The pore sizes of membranes with hexagonal order increased, in the following series: plain BCP membrane < TPA < Ru < AM < DHBA.

ASSOCIATED CONTENT

Supporting Information

Figures S1 and S2 as mentioned in the text. This material is available free of charge via the Internet at http://pubs.acs.org.

AUTHOR INFORMATION

Corresponding Author

*E-mail: suzana.nunes@kaust.edu.sa. Tel.: +966 2 8082771.

Notes

The authors declare no competing financial interest.

ACKNOWLEDGMENTS

The authors thank Dr. Haizhou Yu and Dr. Xiaoyan Qiu for for the protein analysis.

REFERENCES

(1) Jackson, E. A.; Hillmyer, M. A. *ACS Nano* **2010**, *4* (7), 3548−3553.
(2) Chinthamanipeta, P. S.; Lou, Q.; Shipp, D. A. *ACS Nano* **2011**, *5* (1), 450−456.
(3) Li, M; Douki, K; Goto, K.; Li, X.; Coenjarts, C.; Smilgies, D. M.; Ober, C. K. *Chem. Mater.* **2004**, *16*, 3800−3808.
(4) Bates, F. S.; Fredrickson, G. H. *Phys. Today* **1999**, *52*, 32−38.
(5) Vukovic, I.; Voortman, T. P.; Hermida Merino, D.; Portale, G.; Ruokolainen, P. H. J.; Ten Brinke, G.; Loos, K. *Macromolecules* **2012**, *45*, 3503−3512.
(6) Hayward, R. C.; Pochan, D. J. *Macromolecules* **2010**, *43*, 3577−3584.
(7) Ludwigs, S.; Boker, A.; Voronov, A.; Rehse, N.; Magerle, R.; Krausch, G. *Nat. Mater.* **2003**, *2*, 744−747.
(8) Albert, J. N. L.; Epps, T. H. *Mater. Today* **2010**, *13* (6), 24−33.
(9) Elbs, H.; Fukunaga, K.; Stadler, R.; Sauer, G.; Magerle, R.; Krausch, G. *Macromolecules* **1999**, *32*, 1204−1211.
(10) Malenfant, P. R. L.; Wan, J.; Taylor, S. T.; Manoharan, M. *Nat. Nano Tech.* **2007**, *2*, 43−46.
(11) Xu, T.; Stevens, J.; Villa, J. A.; Goldbach, J. T.; Guarini, K. W.; Black, C. T.; Hawker, C. J.; Russell, T. P. *Adv. Funct.Mater.* **2003**, *13*, 698−702.
(12) Cheng, F.; Yang, X.; Peng, H.; Chen, D.; Jiang, M. *Macromolecules* **2007**, *40*, 8007−8014.
(13) Zhulina, E. B.; Borisov, O. V. *Macromolecules* **2012**, *45*, 4429−4440.
(14) Noro, A.; Sageshima, Y.; Arai, S.; Matsushita, Y. *Macromolecules* **2010**, *43*, 5358−5364.
(15) Zhang, L.; Eisenberg, A. *J. Am. Chem. Soc.* **1996**, *118*, 3168−3181.
(16) Cui, H.; Chen, Z.; Wooley, K. L.; Pochan, D. J. *Soft Matter* **2009**, *5*, 1269−1278.
(17) Zhong, S.; Cui, H.; Chen, Z.; Wooley, K. L.; Pochan, D. J. *Soft Matter* **2008**, *4*, 90−93.
(18) Koh, H. D.; Park, S.; Russell, T. P. *ACS Nano* **2010**, *4*, 1124−1130.
(19) Soininen, A. J.; Tanionou, I.; Ten Brummelhuis, N.; Schlaad, H.; Hadjichristidis, N.; Ikkala, O.; Raula, J.; Mezzenga, R.; Ruokolainen, J. *Macromolecules* **2012**, *45*, 7091−7097.
(20) Valkama, S.; Ruotsalainen, T.; Nykanen, A.; Laiho, A.; Kosonen, H.; Ten Brinke, G.; Ikkala, O.; Ruokolainen, J. *Macromolecules* **2006**, *39*, 9327−9336.
(21) Yang, S. Y.; Ryu, I.; Kim, H.; Kim, J. K.; Jang, S. K.; Russell, T. P. *Adv. Mater.* **2006**, *18*, 709−712.
(22) Valkama, S.; Kosonen, H.; Ruokolainen, J.; Haatainen, T.; Torkkeli, M.; Serimaa, R.; Ten Brinke, G.; Ikkala, O. *Nat. Mater.* **2004**, *3*, 872−876.
(23) Van Zoelen, W.; Asumaa, T.; Ruokolainen, j.; Ikkala, O.; Ten Brinke, G. *Macromolecules* **2008**, *41*, 3199−3208.
(24) Van Zoelen, W.; Alberda Van Ekenstein, G.; Ikkala, O.; Ten Brinke, G. *Macromolecules* **2006**, *39*, 6574−6579.
(25) Peinemann, K. V.; Abetz., V.; Simon, P. W. F. *Nat. Mater.* **2007**, *6*, 992−996.
(26) Nunes, S. P.; Karunakaran, M.; Pradeep, N.; Behzad, A. R.; Hooghan, B.; Sougrat, R.; He, H.; Peinemann, K. V. *Langmuir* **2011**, *27*, 10184−10190.
(27) Nunes, S. P.; Behzad, A. R.; Hooghan, B.; Sougrat, R.; Karunakaran, M.; Pradeep, N.; Vainio, U.; Peinemann, K. V. *ACS Nano* **2011**, *5*, 3516−3522.
(28) Nunes, S. P.; Sougrat, R.; Hooghan, B.; Anjum, D. H.; Behzad, A. R.; Zhao, L.; Pradeep, N.; Pinnau, I.; Vainio, U.; Peinemann, K. V. *Macromolecules* **2010**, *43*, 8079−8085.
(29) Marques, D. S.; Vainio, U.; Chaparro, N. M.; Calo, V. M.; Behzad, A. R.; Pitera, J. W.; Peinemann, K. V.; Nunes, S. P. *Soft Matter* **2013**, *9*, 5557−5564, DOI: 10.1039/C3SM27475F.
(30) Qiu, X.; Yu, H.; Karunakaran, M.; Pradeep, N.; Nunes, S. P.; Peinemann, K. V. *ACS Nano* **2013**, *7*, 768−776.
(31) Kuila, B. K.; Gowd, E. B.; Stamm, M. *Macromolecules* **2010**, *43*, 7713−7721.
(32) Peng, H.; Chen, D.; Jiang, M. *J. Phys. Chem. B* **2003**, *107*, 12461−12464.
(33) Roland, S.; Gaspard, D.; Prudhomme, R. E.; Bazuin, C. G. *Macromolecules* **2012**, *45*, 5463−5476.
(34) Donohue, J. *J. Phys. Chem.* **1952**, *56*, 502−510.
(35) Etter, M. C. *J. Phys. Chem.* **1991**, *95*, 4601−4610.
(36) Shattock, T. R.; Arora, K. K.; Vishweshwar, P.; Zaworotko, M. J. *Crystal Growth Des.* **2008**, *8*, 4533−4545.
(37) Almarsson, O.; Zaworotko, M. J. *Chem. Commun.* **2004**, *17*, 1889−1896.
(38) Clodt, J. I.; Rangou, S.; Schröder, A.; Buhr, K.; Hahn, J.; Jung, A.; Filiz, V.; Abetz, V. *Macromol. Rapid Commun.* **2013**, *34*, 190−194.
(39) Dorin, R. M.; Marques, D. S.; Sai, H.; Vainio, U.; Phillip, W. A.; Peinemann, K. V.; Nunes, S. P.; Wiesner, U. *ACS Macro Lett.* **2012**, *1*, 614−617.
(40) Bhatia, S. R.; Mourchid, A.; Joanicot, M. *Curr. Opin. Colloid Interface Sci.* **2001**, *6*, 471−478.
(41) Hyun, K.; Nam, J. G.; Wilhellm, M.; Ahn, K. H.; Lee, S. J. *Rheol. Acta* **2006**, *45*, 239−249.
(42) Buitenhuis, J.; Förster, S. J. *J. Chem. Phys.* **1997**, *107*, 262−272.